IEEE Access
Multidisciplinary ⋮ Rapid Review ⋮ Open Access Journal

Received 3 June 2024, accepted 20 June 2024, date of publication 24 June 2024, date of current version 3 July 2024.

Digital Object Identifier 10.1109/ACCESS.2024.3418623

RESEARCH ARTICLE

Reducing Step Size of Hardware-in-Loop Simulation in Electro-Dynamic Shaker Controller Design by Electrical-Mechanical Analogy

GUOYUAN LIU[1], ZEMIN PAN[2], AND LIANG CHEN[2]
[1]School of Information Science and Engineering, Zhejiang Sci-Tech University, Hangzhou 310018, China
[2]School of Information Science and Engineering, NingboTech University, Ningbo 315100, China

Corresponding author: Liang Chen (21410077@zju.edu.cn)

ABSTRACT Shaker is the key facility of the vibration test system. The wide frequency band of the vibration signal poses a challenge on the shaker controller design, therefore a hardware in loop (HIL) test is desired to verify the controller performance before it is deployed in the real device. The test accuracy depends on the accurate model of the shaker simulated in the HIL simulator, which must be discretized as required by the HIL solver. In this paper, we are going to show that a high resonance peak of the shaker above 1500Hz, which is associated with both the electrical modes and the mechanical modes, can be greatly affected by the step of the discretized model. To overcome the impact of discretization effects on controller validation, this paper utilizes an equivalent model of the shaker derived from the electro-mechanical analogy method, which allows the shaker to be accurately modeled and discretized at a 1μs step in the electrical domain of the HIL402. This provides a solution for the HIL validation of mechatronic systems with high-frequency characteristics, improving the difficulties in modeling such systems in HIL. The effectiveness of the proposed method is verified in both frequency domain test and time domain test under the Typhoon 402 HIL environment.

INDEX TERMS Vibration system, electromechanical simulation model, hardware-in-the-loop (HIL), dual loop controller.

I. INTRODUCTION

Vibration shaker is a device used in laboratory or industrial applications to generate controlled mechanical vibrations, typically for testing the durability, resonant frequencies, or stress responses of materials and components [1], [2], [3], [4]. A vibration shaker typically consists of a coil generating electric force, a mounting table for test specimens, a power electric based amplifier to control the input signal [5], [6], [7], [8], [9]. And due to the construction of the shaker, the typical shaker without control has two lightly damped resonant peaks, one in low frequency band, e.g. < 50 Hz, and the other in high frequency band e.g. > 1000 Hz [10], [11], [12].

Vibration control often uses frequency response compensation to minimize the impact of two lightly damped resonance peaks on the system. Reference [13] proposed an inverse model method to generate the proper feed-forward control signal to alleviate the control effort requirement of the feedback loop in order to avoid the excitation of the resonance. And [14] gives a digital acceleration controller to reach a good response of command tracking at 2 kHz, by using a notch compensator to compensate the amplitude of high frequency resonance and a reference tracking compensator based on the internal model principle to guarantee the good ability of sinusoidal reference tracking. Additionally, in acceleration control, [15] provides a robust disturbance controller whose center frequency is synchronously tuned in accordance with the acceleration reference frequency and the value of weighting factor between (0, 1) reflects the trade-off

The associate editor coordinating the review of this manuscript and approving it for publication was Wen-Sheng Zhao.

© 2024 The Authors. This work is licensed under a Creative Commons Attribution-NonCommercial-NoDerivatives 4.0 License.
For more information, see https://creativecommons.org/licenses/by-nc-nd/4.0/

between the system stability and command traceability to achieve the excellent robustness in the closed loop control from 20 Hz to 200 Hz.

And in vibration control, numerous methods for current control of power amplifiers have also been developed. Reference [16] addresses the deadband time's effect on system performance, using PI and simple deadband control to improve current tracking from 10 to 2000 Hz. Reference [17] overcomes output voltage limitations in traditional PWM modulation with Multidimensional Feedback Quantization Modulation (MDFQM), enabling current control for cascaded shakers.

The effectiveness and feasibility of various complex control methods need to be verified before deployed in the real system. Therefore, the low-cost hardware-in-the-loop (HIL) validation has become an essential part of control verification in power systems. And it's widely applied in multiple fields, encompassing applications in microgrid control, automotive control systems, and active bridge development, among others [18], [19], [20]. Moreover, the model's accuracy greatly influences the performance of the controller. The accuracy of the discretized model is crucial for maintaining the fidelity of real-time HIL simulations [21], [22]. Currently, most HIL vendors provide FPGA-based solutions that allow models to run at microsecond speeds, greatly improving the accuracy of the modeling process [23]. Custom models are limited to the slower ARM side, unlike the FPGA side, potentially causing discrepancies in high-frequency models that can impact controller validation.

To overcome the limitation, this paper utilizes an electrical-mechanical analogy, which mathematically converts the mechanical subsystem of the shaker into an electrical subsystem, and then an equivalent dynamic model of the shaker but containing only the electrical elements can be obtained. This pure electrical model can be well handled by the most FPGA-based HIL solver, consequently the discretization step of shaker can be greatly reduced and the HIL simulation fidelity is improved.

The remainder of this paper is organized as follows. In Sec. II, the shaker model is built in the continuous domain. The Sec. III analyzes the impact of the discretization step on the model discrepancy, and then the electrical-mechanical analogy is applied to derive the equivalent circuit model. In Sec. IV, the shaker controller design is explained and will be tested in HIL environment. The HIL simulation results are analyzed and comparison between the FPGA implementation and the Arm implementation is presented. The Sec. V draws the conclusion.

II. THE COMPLEX ELECTROMECHANICAL OF THE SHAKER

In the vibration system, the power amplifier is used to amplify the command signal from the controller, and the shaker is used to receive the signal and vibrate (as shown in Fig.1). When the shaker receives the output current from the power amplifier, the shaker generates force according to the principle of the Electromagnetic induction, which can be measured by the accelerometer. As the controlled object of the power amplifier, the shaker is equivalent to a voltage source model with a series resistance and inductance in the circuit (as shown in Fig.2). And the controlled source originates from the mechanical movement of the internal coil of the shaker. The electromechanical characteristics of the shaker make the design of the vibration controller very challenging. The description of the symbols in Fig.2 are summarized in Table 1.

Model analysis aids in understanding the characteristics of the shaker. The motion equation of the coil is modelled by (1) according to the Newton's second law. And similarly,

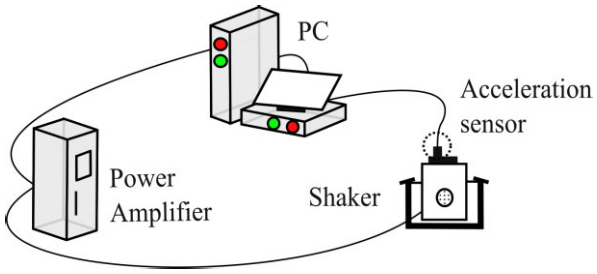

FIGURE 1. The composition of the vibration system.

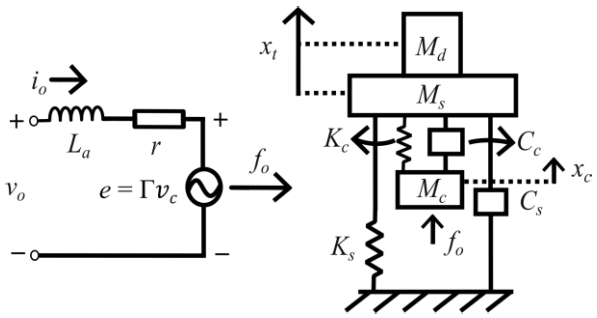

FIGURE 2. The equivalent physical model of the shaker during operation.

TABLE 1. Meaning of character used.

Symbol	Meaning
L_a,r	Coil inductance and resistance
$\Gamma = Bl = f_o/i_o$	Shaker ratio of thrust (f_o) to coil current (i_o)
M_c, M_s, M_d, and M	Coil mass, table mass, specimen mass, and total mass ($M = M_c+M_s+M_d$)
C_c, C_s	Coil damping coefficient, shaker suspension damping coefficient
K_c, K_s	Coil stiffness coefficient, shaker suspension stiffness coefficient
x_t, x_c, and v_c	Table displacement, coil displacement, and coil velocity

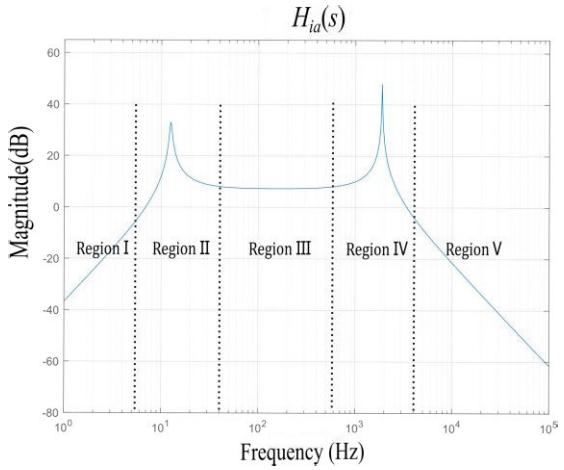

FIGURE 3. Vibration table fourth-order $H_{ia}(s)$ characteristic amplitude frequency response.

TABLE 2. Parameters of the investigated vibration shaker.

Parameters	Symbol	Value
Coil inductance[1]	L_a	138 (μH)
Resistor[1]	r	4 (Ω)
Coil mass	M_c	0.2587 (kg)
Shaker table mass	M_s	0.1335 (kg)
Coil stiffness coefficient	K_c	$3.1977 \cdot 10^7$ (N/m)
Coil damping coefficient	C_c	24.4543 (N·sec/m)
Suspension stiffness coefficient	K_s	$8.7542 \cdot 10^3$ (N/m)
Suspension damping coefficient	C_s	5.6756 (N·sec/m)
Force generation constant	Γ	3.2332 (N/A)

Coil inductance[1] and Resistor[1] are assumed to be constant and equivalent to the value measured at 2 kHz.

the motion equation of the table is modelled by (2).

$$\Gamma i_o = K_c\,(x_c - x_t) + C_c s\,(x_c - x_t) + M_c s^2 x_c \tag{1}$$

$$K_c\,(x_c - x_t) + C_c s\,(x_c - x_t) = K_s x_t + C_c s x_t + (M_d + M_s)\,s^2 x_t \tag{2}$$

Combine (1) and (2), the transfer function from coil current to the specimen acceleration can be modelled by $H_{ia}(s)$ shown in (3)

$$H_{ia}(s) = \frac{\Gamma(C_C s + K_C)s^2}{M_c\,(M_d + M_s)\,s^4 + (M_c C_S + C_C M)\,s^3 + (M_c K_S + C_C C_S + K_C M)\,s^2 + (C_C K_S + K_C C_S)\,s + K_C K_S} \tag{3}$$

If the power amplifier is controlled as a high bandwidth current source, then the plant model of the shaker can be modelled by the fourth-order dynamic system as (3).

Alternatively, the power amplifier can also be considered as a voltage source where its terminal voltage v_o is regarded as the input signal of the shaker system. In this case, the shaker model can be obtained as (4).

$$H_{shaker}(s) = \frac{1}{sL_a + r} H_{ia}(s) \tag{4}$$

A typical $H_{ia}(s)$ frequency response is illustrated in Fig.3 where two lightly damped resonant peak can be observed in region II and region IV respectively. The parameters we used in this paper of the EDS-045 shaker model which is manufactured by the Donglingtech are listed in Table 2.

Usually, it is required that the frequency component of the stimulated acceleration signal covers the band from region II to region IV [12]. Moreover, it should be noted that the frequency of these peaks varies with the load mass according to (3). Therefore, the shaker controller must be carefully designed to achieve a wide control bandwidth while avoiding the excitation of these two modes. In the other words, to valid the shaker controller algorithm in a HIL platform, the frequency response characteristic of the shaker must be modelled with high fidelity, especially for the resonant peaks.

III. DISCRETIZATION OF THE SHAKER MODEL

A. DISCRETIZATION OF SHAKER STATE-SPACE EQUATION MODELS

To build a time domain simulation model, the transfer function (3) is converted as a state model in the form of (5).

$$\begin{cases} \dot{x} = Ax + Bu \\ y = Cx \end{cases} \tag{5}$$

Then (5) is further discretized as (6) using Tustin method to preserve the accuracy of the frequency response in high frequency domain.

$$\begin{cases} x(k+1) = \dfrac{2 + AT_s}{2 - AT_s} x(k) + \dfrac{BT_s}{2 - AT_s} u(k) \\ y(k) = Cx(k) \end{cases} \tag{6}$$

The impact of the discretization step size on the frequency response characteristic of the discretized shaker model is demonstrated in Fig.4, where the frequency response of the original continuous model, discretized models of the step size 1 μs, 50 μs, and 100 μs are compared. It is observed in Fig.4 (a) that the step size has no impact on model frequency response in low frequency band, where the low frequency resonant peak is the same for three different step size settings. However, in the high frequency band, the differences of frequency responses among these models are noticeable. Though it is inevitable that there will be a discrepancy in the frequency response between the continuous model and the discretized mode, our most interested is how the high frequency resonant peak is modelled.

From Fig.4 (b) and Fig.4 (c), it is shown that the model discretized at 1 μs step size can model the resonant peak accurately. On the other hand, the model discretized at 50 μs

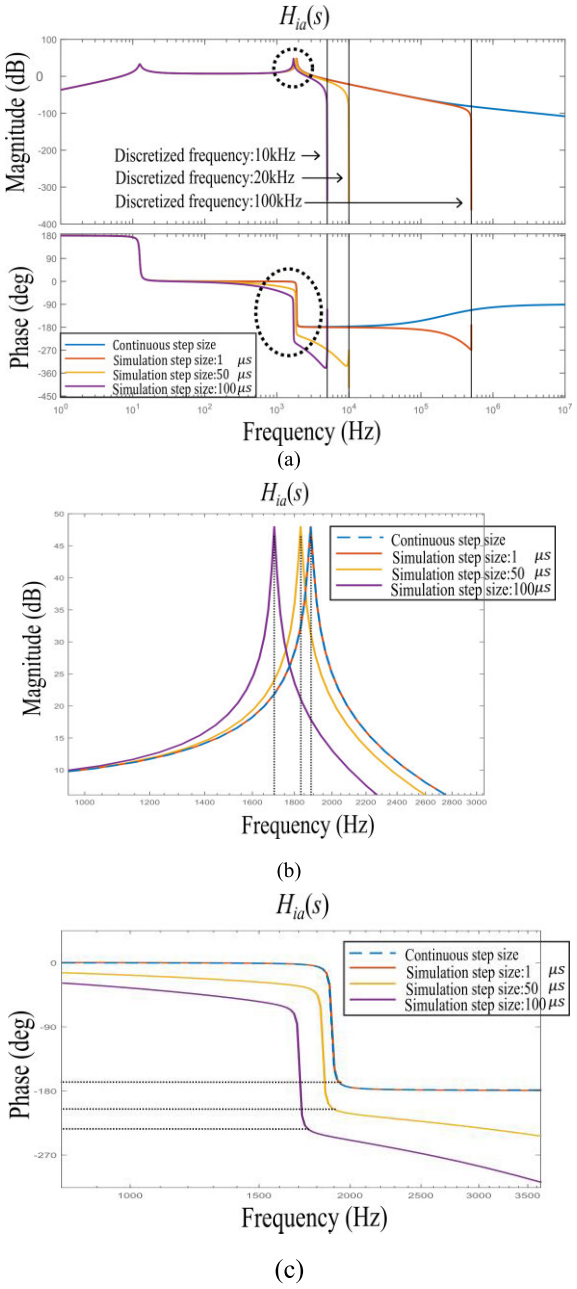

FIGURE 4. Influence of different discretization steps on discrete model constructed by state space equation. (a) is frequency response plots for model differences. (b) is the circle magnification plot of amplitude frequency response in (a). And (c) is the circle magnification plot of phase frequency response in (a).

step size and 100 μs step size have large deviation on both amplitude response and phase response. The phase response is more critical because the large phase lagging caused by the discretization makes the phase of the models less than -180 degree around the peaks, which could cause unrealistic stability problem when such models are used in the HIL simulation.

After addressing the importance of the choosing a small enough discretization step size, we are going to present how

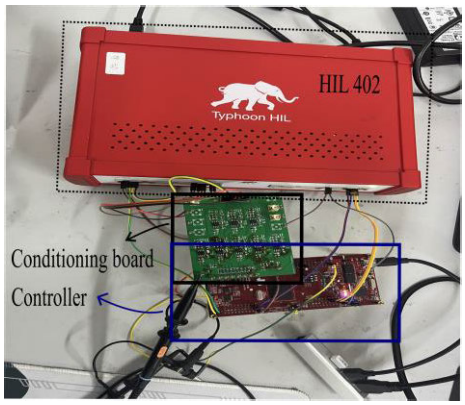

FIGURE 5. HIL experiment connection diagram. In this figure, the DSP controller F28379d is the proposed dual loop controller. And the conditioning board is used for conditioning and scaling signals.

TABLE 3. The mechanical parameters are equivalent to the circuit characteristics by converting force into current.

Mechanical parameters	Symbol	Electrical characteristic	Symbol
Force	f	Current	i
Velocity	v	Voltage	e
Lubricity (Inverse friction)	$1/B$	Resistance	R
Mass	M	Capacitance	C
Compliance (Inverse spring constant)	$1/K$	Inductance	L

we can simulate shaker model at 1 μs on the Typhoon 402 platform, which is shown in Fig.5. The customize shaker model (6), which contains both mechanical elements and the electrical elements, is not directly supported officially in the FPGA side. Nevertheless, as discussed above, running the shaker model at the Arm side, whose minimal achievable time step is at the scale of 100 μs according to our test, could simulate an inaccurate response or even instability.

Since the official FPGA solver supports only the electrical elements, we are going to convert the mechanical part of the shaker model into an equivalent electrical circuit model, which will be elaborated in the next section.

B. DERIVATION OF ELECTRICAL CIRCUIT MODEL OF SHAKER

According to the Linear Physical Systems Analysis [24], the mechanical system can be modeled by system analogy. The mapping relationship between the mechanical quantity and the electrical quantity is summarized in Table 3. The mapping relationship between mechanical equation and electrical equation can be subsequently obtained, as summarized in Table 4.

Based on these mappings, the mechanical of the shaker (1) and (2) can be converted as an equivalent model, expressed

TABLE 4. Electrical equation and mechanical equation transformation.

Mechanical equation	Electrical equation
Velocity, $v = f/B$	Voltage, $e = iR$
Velocity, $v = df/Kdt$	Voltage, $e = Ldi/dt$
Velocity, $v = \int(fdt)/M$	Voltage, $e = \int idt/C$
Force, $f = K\int(vdt) = Kx$	Current, $i = \int edt/L$
Force, $f = Mdv/dt$	Current, $i = Cde/dt$

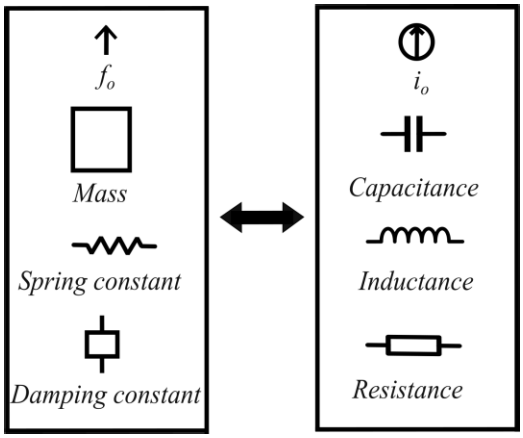

FIGURE 6. The electromechanical analogy method, where force is converted into current.

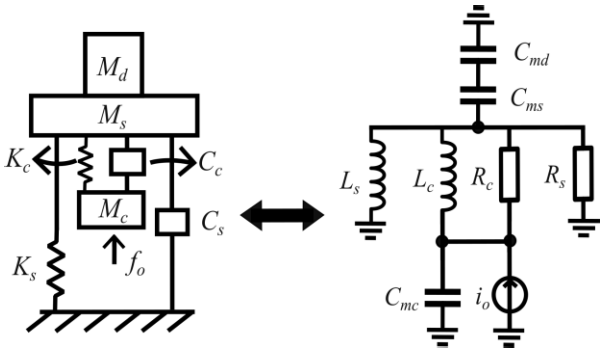

FIGURE 7. The derived electrical circuit model of the shaker.

TABLE 5. The parameter of the electrical circuit model.

Symbol	Value
C_{mc}	0.2857 (F)
C_{md}	1 (F)
C_{ms}	0.1335 (F)
C_{mls}	1.1335 (F)
R_c	0.0409 (Ω)
R_s	0.1762 (Ω)
L_c	$3.1272 \cdot 10^{-8}$ (H)
L_s	$1.1423 \cdot 10^{-4}$ (H)

as (7) and (8). By using equations (9) and (10), equations (7) and (8) can be simplified to obtain equations (11) and (12).

Fig.6 and Fig.7 present the model derived using the electromechanical analogy method.

$$\Gamma i_o = C_{mc} e_c s + \left(\frac{1}{R_c} + \frac{1}{sL_c}\right)(e_c - e_t) \tag{7}$$

$$\left(\frac{1}{R_c} + \frac{1}{sL_c}\right)(e_c - e_t) = (C_{md} + C_{ms})\, e_t s + (\frac{1}{R_s} + \frac{1}{sL_s}) e_t \tag{8}$$

$$Y_1 = \frac{1}{R_c} + \frac{1}{sL_c} \tag{9}$$

$$Y_2 = \frac{1}{R_s} + \frac{1}{sL_s} \tag{10}$$

$$\Gamma i_o = C_{mc} e_c s + Y_1 (e_c - e_t) \tag{11}$$

$$Y_1 (e_c - e_t) = ((C_{md} + C_{ms})\, s + Y_2)\, e_t \tag{12}$$

The circuit of system (11) and (12) is illustrated in Fig.7. The topology of the derived model performs the mechanical characteristic of the shaker. Table 5 shows the parameters of the derived model. Capacitance C_{mc}, C_{md}, C_{ms} represent the coil mass, specimen mass and table mass respectively. And $C_{mls} = C_{md} + C_{ms}$. Resistance R_c and R_s represent the inverse friction constant of the coil and the table suspension respectively. Inductance L_c and L_s represent the reverse stiffness coefficient of the coil and the shaker suspension respectively. Voltage e_c and e_t represent the coil motion speed and the table motion speed, respectively.

In Fig.8, the input signal of the converted shaker model is i_o, which is the generated by the power amplifier. The specimen acceleration a_t which will be feedback to the shaker controller is modelled by scaling the $1/C_{mls}$ times of the inductor current i_t value. And, the back electromotive force e which is going to the electrical characteristic of shaker, is modelled by scaling the Γ times of the capacitance C_{mc} voltage value. The delay between the Typhoon HIL's interfaces is negligible for their step size is the same.

Theoretically, the specimen acceleration a_t and the back voltage e which is also as the feedback signal of the controller, can be modelled in electric domain of Typhoon HIL through this model. In support of the theoretical aspect, we are going to sweep frequency to the model in the next section.

C. VERIFICATION OF ELECTRICAL CIRCUIT MODEL OF SHAKER

The frequency response from the sweep test is compared with the Simulink model's to validate its accuracy. The derived model with the step size of 1 μs, and the state-space equation model with the step size of 100 μs, are constructed in the HIL 402. The sweep experiment continuously sends signals to the

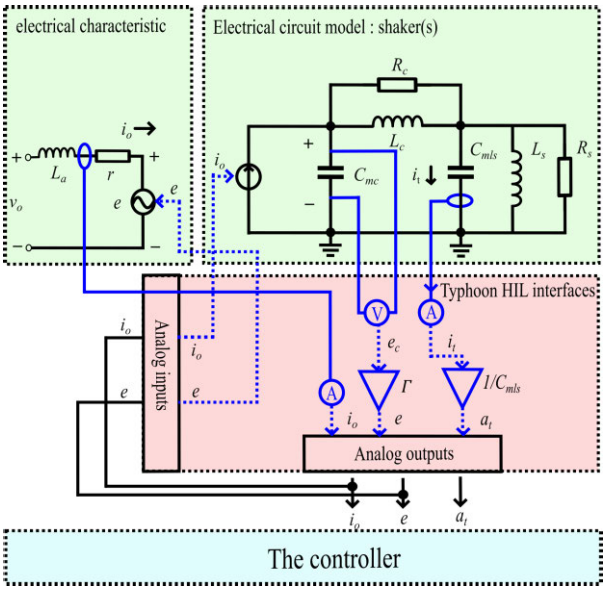

FIGURE 8. Deployment of the shaker equivalent model in HIL.

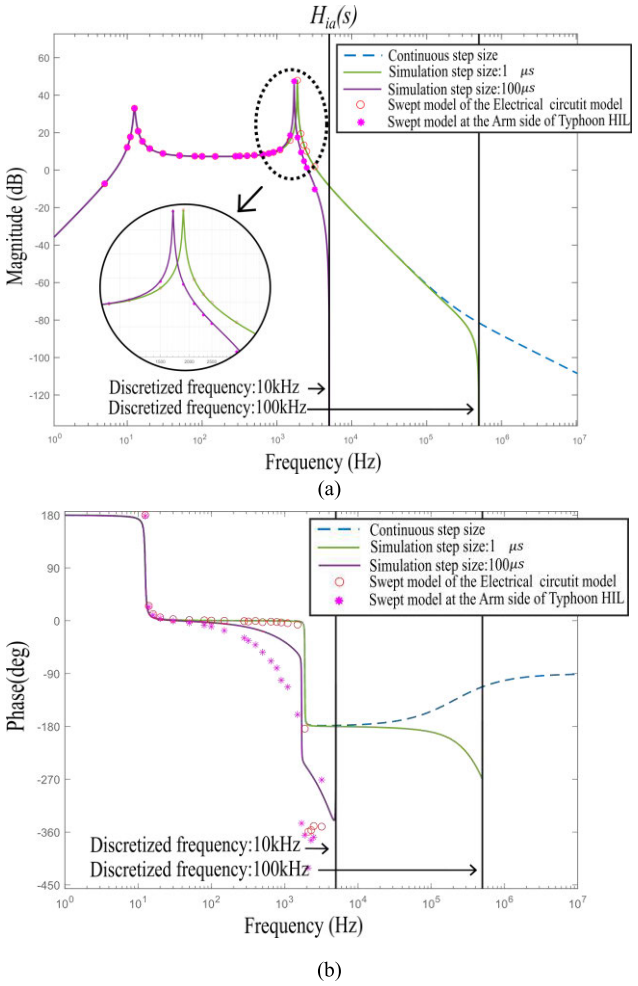

FIGURE 9. Swept frequency response of the shaker models. (a) shows the amplitude frequency response of different model. (b) shows the phase frequency response of different model.

shaker model through the 402 simulator, and the collected signal ratio obtains the sweep data points, as shown in Fig.9.

Fig.9 compares two swept model mentioned above and their theoretical model which is built and discretized in Simulink. And we can see that these models behave the same in the low frequency of the shaker, which is in line with the theoretical analysis in Sec. II.

From Fig.9 (a), The frequency responses of the two swept model are in line with their Simulink theoretical model respectively. And at high frequency, the amplitude difference between the two swept model is the same with the difference between the discretized Simulink model of the step size 1 μs and 100 μs.

And From Fig.9 (b), it is shown that, the phase frequency response of the swept electrical circuit model is consistent with the discretized theoretical one. However, the phase frequency of the swept other model appears larger phase deviation compared its discretized Simulink model, especially at 1 kHz. This suggests that, the model built at the Arm side of Typhoon HIL could cause unrealistic stability problem comparing with the electrical circuit model.

After validating the reliability of the electrical circuit model alone, we are going to present, how to use this model in Typhoon HIL to validate the performance of the controller in the Sec. IV.

IV. CLOSED-LOOP HIL EXPERIMENTS

In the previous sections, we have demonstrated the discretization method of the shaker plant model will influence its accuracy in HIL. In this section, we will demonstrate that the proper discretization method is critical when we evaluate the shaker controller in HIL. Firstly, the shaker controller algorithm will be briefly introduced. Fig.10 is the schematic diagram of the vibration control system powered by the current type switching power amplifier.

A. DUAL LOOP CONTROLLER

From Fig.10, it's shown that in the dual loop controller, the current reference signal is given by the outer loop of the acceleration controller. The preceding power amplifier is equivalent to a nominal gain K_{pa} in the controller. The unipolar modulation is applied. The DC-link voltage V_{dc} is 950 V. The rated output current of the amplifier is 15 A. A 0.012 H filter L_1 is added between power amplifier and the shaker to improve the current quality. The sampling frequency of the dual loop controller is 50 kHz, the switching frequency is 20 kHz. The control bandwidth of acceleration reference signal tracking is 40∼500 Hz.

1) Current loop controller. The model of the power amplifier is expressed as (13).

$$\frac{i_o}{v_{pwm} - e} = \frac{1}{r + s(L_a + L_1)} \tag{13}$$

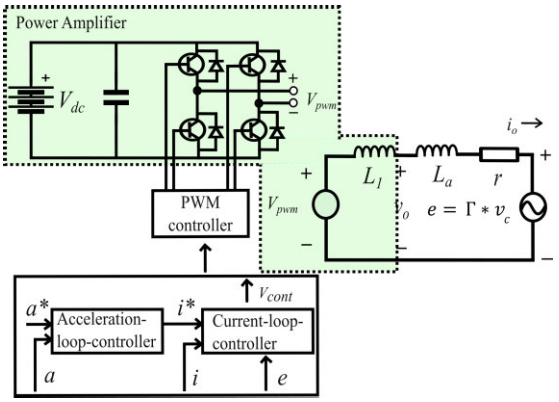

FIGURE 10. Vibration control system powered by the power amplifier in the current source mode.

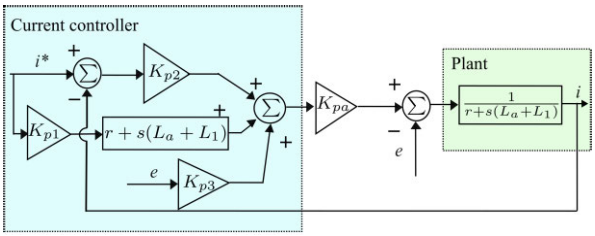

FIGURE 11. Current loop controller.

Based on the inverse model method, the inner current loop controller is designed, which is shown in Fig.11. In Fig.11, K_{p1} is the gain tuning the inverse model gain, will boost the reference tracking bandwidth in a feed-forward manner. K_{p2} sets the feedback gain. K_{p3} sets the disturbance rejection gain.

2) Acceleration loop controller. The low frequency resonance peaks can be accurately compensated by using the method of inversing the model. High frequency resonance peak is usually compensated by a notch filter.

(14) is the low frequency resonance peak compensator [14]. The pole μ_1 determines the bandwidth of the compensator. And it can accurately compensate the low frequency resonance peak by appropriately moving the pole.

$$G_{LF}(s) = \frac{\left[Ms^2 + C_S s + K_S\right] r + \Gamma^2 s}{K_{pa}\Gamma(\mu_1 s + 1)^2}\mu_1^2 \tag{14}$$

The high frequency notch filter is expressed as (15), where D_m is a design parameter that determines the bandwidth [13], and other two parameter w_p and e_p are associate with the mechanical parameters of shaker as expressed in (16) and (17). Fig.12 is the diagram of the acceleration loop design. Similarly, K_{p4} sets the feedback gain. The values of the dual loop controller parameter used in this paper are listed in Table 6.

$$G_{HF}(s) = \frac{s^2 + 2e_p\omega_p s + \omega_p^2}{s^2 + 2D_m\omega_p s + \omega_p^2} \tag{15}$$

$$\omega_p = \sqrt{\frac{(M_d + M_s + M_c)K_c}{(M_d + M_s)M_c}} \tag{16}$$

$$e_p = \frac{C_C}{2}\sqrt{\frac{(M_d + M_s + M_c)}{(M_d + M_s)\,M_c K_c}} \tag{17}$$

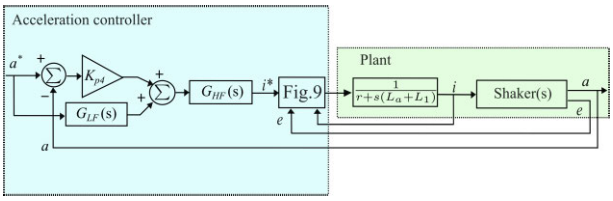

FIGURE 12. Acceleration loop controller.

TABLE 6. Parameters of dual loop controller.

Parameters	Symbol	Value
The nominal gain of power amplifier	K_{pa}	3.5
The inverse model gain in current loop	K_{p1}	0.2857
The feedback gain in current loop	K_{p2}	30
The disturbance rejection gain in current loop	K_{p3}	0.2857
The feedback gain in acceleration loop	K_{p4}	0.001
The pole of $G_{LF}(s)$)	μ_1	0.69
Damping coefficient of $G_{HF}(s)$	D_m	0.25

For the purpose of analysing the performance of the dual loop controller, we are going to present the closed-loop response of the dual loop controller in the next section.

B. CLOSED-LOOP PERFORMANCE ANALYSIS OF THE DUAL LOOP CONTROLLER

Fig. 13 displays the closed-loop response of the dual-loop controller, illustrating the scenarios when the shaker plant model built as a continuous model and when it is represented by discretized models with step sizes of 1 μs and 100 μs, respectively. It's observed in Fig.13 that the closed loop response of the continuous model and 1μs step size model are identical, which indicating that 1 μs step size model can evaluate the dual loop controller performance accurately. On the other hand, the model with a 100 μs step size demonstrates a distinctive behavior in the closed-loop performance of the dual loop controller, characterized by a significant spike in magnitude and greater phase decay. Specifically, at 1.664 kHz—delineated by line ABC in Fig. 13—the 100 μs step size model exhibits a misleading amplitude response of 24.6 dB, which is substantially higher than the 8.6 dB amplitude response observed with the accurate model. This discrepancy in peak response may erroneously lead to controller saturation or even instability during Hardware-in-the-Loop (HIL) simulation, issues that would not arise under correct modeling conditions.

C. HIL EXPERIMENTS WITH THE ELECTRICAL CIRCUIT MODEL

Fig.14 illustrates the interface between the shaker model in the HIL simulator and the DSP controller. The block

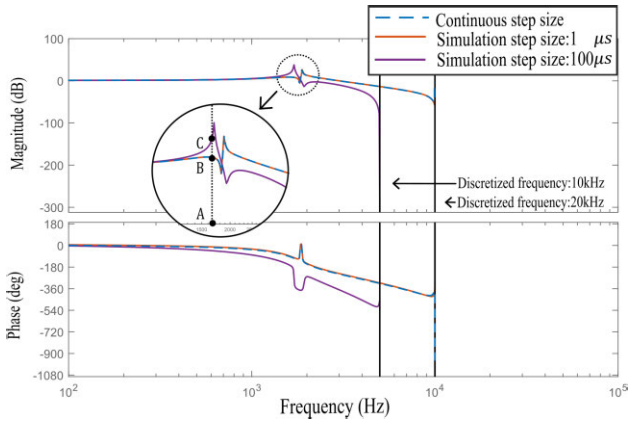

FIGURE 13. Closed loop frequency response of dual loop controller with different shaker models.

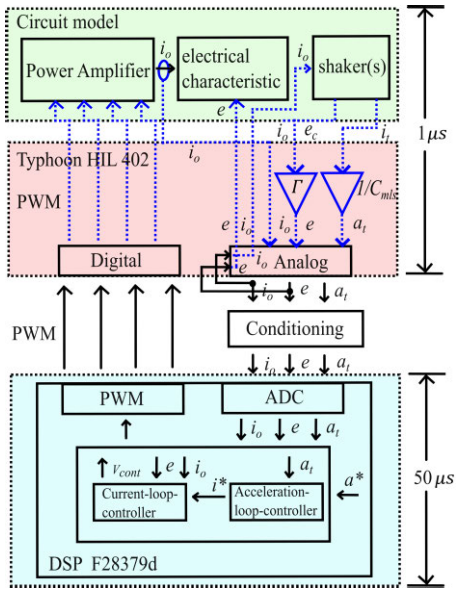

FIGURE 14. The closed loop diagram of the HIL experiment.

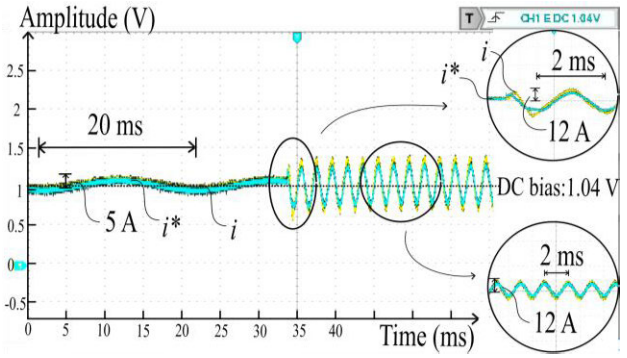

FIGURE 15. Current loop response when the command changes.

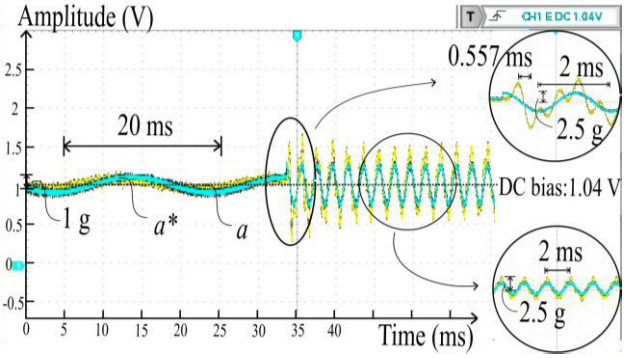

FIGURE 16. Acceleration response during command bursts.

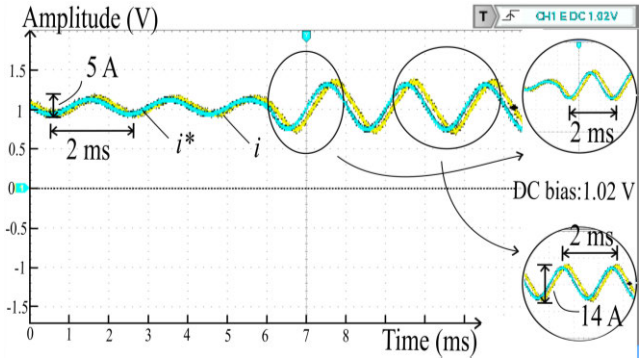

FIGURE 17. The current response when the acceleration command suddenly changes from 1g to 3g.

"Shaker(s)" is discretized at 1 μs in FPGA side thanks to the equivalent circuit model we derived in Sec. III-B.

As shown in Fig.15, when the acceleration reference is switched from 1 g (where g = 9.8 m/s^2) 50 Hz sine wave to 2.5 g 500 Hz, the inner current loop can track the reference within 10 ms and have negligible steady state error.

The response of the outer loop is illustrated in Fig.16. The acceleration reference tracking has negligible steady state error in 50 Hz reference signal. For 500 Hz reference signal, even though the fundamental component of the feedback signal follows the 500 Hz reference, there are noticeable high frequency oscillation. The high frequency oscillation is the 1.79 kHz component caused by the high frequency peak. The response matches the analytical analysis in Fig.13, that the evaluated dual loop controller can track the reference signal stably, but the resonance caused by the high frequency peak can be further mitigated by fine tuning the high frequency notch filter (14).

Fig.17 and Fig.18 respectively show the dual-loop response when the acceleration command abruptly changes from 1g to 3g. It can be clearly seen that the dual-loop response is extremely stable, with rapid responsiveness and strong robust tracking of commands, regardless of whether it is before, during, or after the abrupt change in the acceleration amplitude command.

Comparing Fig.16 and Fig.18, it's apparent that high-frequency interference in acceleration control only occurs during sudden changes in the acceleration frequency

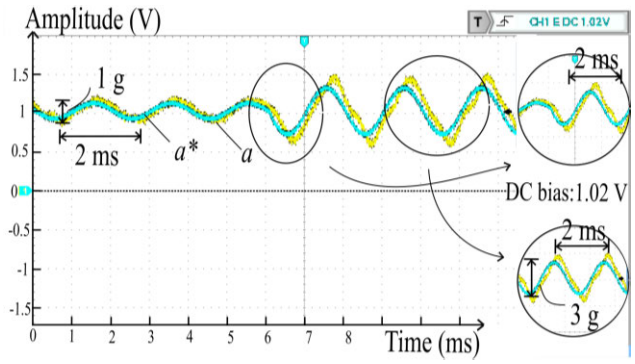

FIGURE 18. The acceleration response when the acceleration command suddenly changes from 1g to 3g.

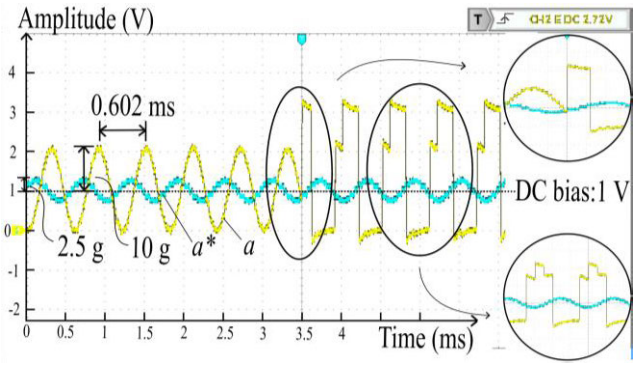

FIGURE 19. Acceleration response when switching the model.

command. The source of this high-frequency interference is the excessive use of differentiators in the controller, rather than the P controller. Differentiators can easily amplify high-frequency signals that are not completely filtered out. This issue can be addressed by fine-tuning Equation (15) during practical controller application.

Moreover, we can verify the impact of model accuracy on controller performance by switching models at high frequencies. Fig.19 shows that when the initial shaker model, built on the FPGA side to track a 1664Hz signal, is switched to the model built on the ARM side, excitation resonance causes the feedback system to severely saturate, preventing the generation of a 1664 Hz sine wave. This actual phenomenon is consistent with the theoretical analysis in Simulink (as shown in Fig.13).

When the shaker is accurately modeled on the FPGA side, the controller maintains stable operation with an 8.6dB amplification. In contrast, when confronted with the inaccurate model built on the ARM side, the controller encounters undesirably elevated amplitude and significant phase reduction, severely compromising system stability.

V. CONCLUSION

For effective validation of controller performance within a HIL environment, it is necessary to discretize the shaker model. However, the challenge arises with commercial HIL FPGA solvers that operate at 1 μs step size and are primarily designed for electrical circuit modeling. These FPGA solvers cannot be directly utilized to accurately capture the high-frequency characteristics of the shaker due to its intrinsic mechanical structure. But in the same time, building the shaker model on the Arm side at 100 μs step size might lead to inaccuracies in evaluating the controller's performance at high frequencies, potentially resulting in misleading outcomes due to the discretization effect.

This paper successfully tackles this problem by translating the mechanical components of the shaker into an equivalent circuit representation. This approach allows the model to be implemented on the FPGA side of the Typhoon HIL system using a precise 1 μs step size. Such a strategy ensures a more accurate modeling of the shaker's high-frequency behavior, thereby facilitating a more reliable assessment of controller performance in the HIL environment.

This paper exemplifies the effective application of the electromechanical analogy method for HIL validation in vibration control. It offers a novel approach for HIL validation of electromechanical systems, particularly those involving high-frequency characteristic modeling. The proposed methodological strategy also holds promising prospects for widespread application in fields such as modeling and HIL validation for automotive control systems.

REFERENCES

[1] L. Yan and C. Zhang, "Shaking-table test and finite element simulation of a novel friction energy-dissipating braced frame," *Buildings*, vol. 14, no. 2, p. 390, Feb. 2024, doi: 10.3390/buildings14020390.

[2] V. M. Vatnik, T. I. Karimov, R. I. Solnitsev, V. Y. Ostrovskii, and M. V. Kulagin, "Signal pre-distortion for vibration table frequency response compensation," in *Proc. Conf. Russian Young Researchers Electr. Electron. Eng. (ElConRus)*, Saint Petersburg, Russia, Jan. 2022, pp. 904–907, doi: 10.1109/ElConRus54750.2022.9755760.

[3] M.-T. Peng and T. J. Flack, "Numerical analysis of the coupled circuit and cooling holes for an electromagnetic shaker," *IEEE Trans. Magn.*, vol. 41, no. 1, pp. 47–54, Jan. 2005, doi: 10.1109/TMAG.2004.840181.

[4] J. Martino and K. Harri, "Virtual shaker modeling and simulation, parameters estimation of a high damped electrodynamic shaker," *Int. J. Mech. Sci.*, vol. 151, pp. 375–384, Feb. 2019, doi: 10.1016/j.ijmecsci.2018.11.025.

[5] T.-H. Chen and C.-M. Liaw, "Vibration acceleration control of an inverter-fed electrodynamic shaker," *IEEE/ASME Trans. Mechatronics*, vol. 4, no. 1, pp. 60–70, Mar. 1999.

[6] H.-C. Chen and J.-Y. Liao, "Digital implementation of GaN-based inverter for permanent magnet electrodynamic shaker," in *Proc. 1st Int. Future Energy Electron. Conf. (IFEEC)*, Taiwan, Nov. 2013, pp. 252–258, doi: 10.1109/IFEEC.2013.6687512.

[7] C.-M. Liaw, W.-C. Yu, and T.-H. Chen, "Random vibration test control of inverter-fed electrodynamic shaker," *IEEE Trans. Ind. Electron.*, vol. 49, no. 3, pp. 587–594, Jun. 2002, doi: 10.1109/TIE.2002.1005384.

[8] Y. Uchiyama and M. Fujita, "Application of two-degree-of-freedom control to electrodynamic shaker using adaptive filter based on H∞ filter," in *Proc. Eur. Control Conf. (ECC)*, Cambridge, U.K., Sep. 2003, pp. 1626–1631, doi: 10.23919/ECC.2003.7085196.

[9] F. Cao, M. Niu, B. Xie, W. Hu, and B. Yang, "Electrical-magnetic-mechanical modeling of a novel vibration shaker based on a rotary permanent magnet," in *Proc. 5th Int. Conf. Mech., Automot. Mater. Eng. (CMAME)*, Guangzhou, China, Aug. 2017, pp. 86–91, doi: 10.1109/CMAME.2017.8540150.

[10] Z. Yan, H. E. Taha, and T. Tan, "Nonlinear characteristics of an autoparametric vibration system," *J. Sound Vib.*, vol. 390, pp. 1–22, Mar. 2017, doi: 10.1016/j.jsv.2016.12.003.

[11] B. Lütkenhöner, "What the electrical impedance can tell about the intrinsic properties of an electrodynamic shaker," *PLoS ONE*, vol. 12, no. 3, Mar. 2017, Art. no. e0174184, doi: 10.1371/journal.pone.0174184.
[12] G. F. Lang and D. Snyder, "Understanding the physics of electrodynamic shaker performance," *Sound Vib.*, no. 10.
[13] L. Martini, "Real-time control of an electrodynamic shaker," Tech. Rep.
[14] L. Della Flora and H. A. Gründling, "Time domain sinusoidal acceleration controller for an electrodynamic shaker," *IET Control Theory Appl.*, vol. 2, no. 12, pp. 1044–1053, Dec. 2008, doi: 10.1049/iet-cta:20080188.
[15] J. Han, T. Tang, and X. Wang, "Sinusoidal vibration test control of a switching mode power amplifier-fed electrodynamic shaker," in *Proc. 1st IEEE Conf. Ind. Electron. Appl.*, Singapore, May 2006, pp. 1–5, doi: 10.1109/ICIEA.2006.257204.
[16] H.-C. Chen, Y.-C. Lin, and J.-Y. Liao, "DSP-based current control with dead-time compensation for full-bridge-fed permanent-magnet electrodynamic shaker," in *Proc. 27th Annu. IEEE Appl. Power Electron. Conf. Expo. (APEC)*, Orlando, FL, USA, Feb. 2012, pp. 2145–2152, doi: 10.1109/APEC.2012.6166118.
[17] H.-C. Chen, C.-Y. Lu, and C.-C. Yao, "Application of multi-dimensional feedback quantized modulation to inverter-fed two cascaded electrodynamic shakers," in *Proc. 41st Annu. Conf. IEEE Ind. Electron. Soc. (IECON)*, Yokohama, Japan, Nov. 2015, pp. 56–61, doi: 10.1109/IECON.2015.7392076.
[18] M. A. Aslam, S. A. R. Kashif, M. Adeel, M. U. Shahid, M. Iqbal, and M. A. Riaz, "A controller hardware in loop framework for microgrid control applications," in *Proc. 6th Int. Conf. Energy Conservation Efficiency (ICECE)*, Lahore, Pakistan, Mar. 2023, pp. 1–5, doi: 10.1109/ICECE58062.2023.10092516.
[19] G. Arena, G. Aiello, G. Scelba, M. Cacciato, and F. Gennaro, "A cost-effective hardware in the loop implementation of dual active bridge for fast prototyping of electric vehicles charging controls," in *Proc. 23rd Eur. Conf. Power Electron. Appl. (EPE ECCE Europe)*, Ghent, Belgium, Sep. 2021, pp. P.1–P.10, doi: 10.23919/EPE21ECCEEurope50061.2021.9570652.
[20] M. Kaczmarek and P. Koralewicz, "Hardware in the loop simulations of industrial application using system on the chip architecture," in *Proc. Int. Conf. Signals Electron. Syst. (ICSES)*, Kraków, Poland, Sep. 2016, pp. 157–160, doi: 10.1109/ICSES.2016.7593842.
[21] E. Liegmann, A. Riccobono, and A. Monti, "Wideband identification of impedance to improve accuracy and stability of power-hardware-in-the-loop simulations," in *Proc. IEEE Int. Workshop Appl. Meas. Power Syst. (AMPS)*, Aachen, Germany, Sep. 2016, pp. 1–6, doi: 10.1109/AMPS.2016.7602873.
[22] F. Mihalič, M. Truntič, and A. Hren, "Hardware-in-the-loop simulations: A historical overview of engineering challenges," *Electronics*, vol. 11, no. 15, p. 2462, Aug. 2022, doi: 10.3390/electronics11152462.
[23] C. Dufour, S. Cense, V. Jalili-Marandi, and J. Belanger, "Review of state-of-the-art solver solutions for HIL simulation of power systems, power electronic and motor drives," in *Proc. 15th Eur. Conf. Power Electron. Appl. (EPE)*, Sep. 2013, pp. 1–12, doi: 10.1109/EPE.2013.6632001.
[24] S. B. Julius and G. P. Allan, *Random Data: Analysis and Measurement Procedures*, 4th ed. Hoboken, NJ, USA: Wiley, 2010.

GUOYUAN LIU was born in Yulin, China, in 1998. She is currently pursuing the master's degree with the School of Information Science and Engineering, Zhejiang Sci-Tech University. Her research interests include shaker table control and full bridge inverter control.

ZEMIN PAN was born in Ningbo, China, in 1987. He received the B.S. and Ph.D. degrees from the Department of Mechanical Manufacture and Automation, Zhejiang University, Hangzhou, China, in 2016.

He has been with NingboTech University, since 2016. He is currently an Associate Professor. His research interests include aircraft digital assembly systems and control techniques, and motion control and adaptive control of electromechanical systems.

LIANG CHEN received the Ph.D. degree from Zhejiang University, Hangzhou, China, in 2020. He joined NingboTech University as a Lecturer, in 2022. His research interests include grid-connected converter control and AC motor drivers.